Sub-50 fs diode-pumped SESAM mode-locked Yb:SrF2 laser

Wen-Ze Xue, Pavel Loiko, Zhang-Lang Lin, Huang-Jun Zeng, Ge Zhang, Abdelmjid Benayad, Simone Normani, Patrice Camy, Xavier Mateos, Valentin Petrov, et al.

Research Article | Vol. 31, No. 10 / 8 May 2023 / Optics Express 16634
Optics EXPRESS

Sub-50 fs diode-pumped SESAM mode-locked Yb:SrF_2 laser

WEN-ZE XUE,[1,2] PAVEL LOIKO,[3] ZHANG-LANG LIN,[1,2] HUANG-JUN ZENG,[1] GE ZHANG,[1,2] ABDELMJID BENAYAD,[3] SIMONE NORMANI,[3] PATRICE CAMY,[3] XAVIER MATEOS,[4] VALENTIN PETROV,[5] LI WANG,[5] AND WEIDONG CHEN[1,2,5,*]

[1]*Fujian Institute of Research on the Structure of Matter, Chinese Academy of Sciences, 350002 Fuzhou, China*
[2]*College of Chemistry and Materials Science, Fujian Normal University, 350002 Fuzhou, China*
[3]*Centre de Recherche sur les Ions, les Matériaux et la Photonique (CIMAP), UMR 6252 CEA-CNRS-ENSICAEN, Université de Caen, 6 Boulevard Maréchal Juin, 14050 Caen Cedex 4, France*
[4]*Universitat Rovira i Virgili, URV, Física i Cristal·lografia de Materials i Nanomaterials (FiCMA-FiCNA)-Marcel·lí Domingo 1, 43007 Tarragona, Spain*
[5]*Max Born Institute for Nonlinear Optics and Short Pulse Spectroscopy, Max-Born-Str. 2a, 12489 Berlin, Germany*
[*]*chenweidong@fjirsm.ac.cn*

Abstract: We report on sub-50 fs pulse generation from a passively mode-locked Yb:SrF_2 laser pumped with a spatially single-mode, fiber-coupled laser diode at 976 nm. In the continuous-wave regime, the Yb:SrF_2 laser generated a maximum output power of 704 mW at 1048 nm with a threshold of 64 mW and a slope efficiency of 77.2%. A continuous wavelength tuning across 89 nm (1006 – 1095 nm) was achieved with a Lyot filter. By implementing a SEmiconductor Saturable Absorber Mirror (SESAM) for initiating and sustaining the mode-locked operation, soliton pulses as short as 49 fs were generated at 1057 nm with an average output power of 117 mW at a pulse repetition rate of ~75.9 MHz. The maximum average output power of the mode-locked Yb:SrF_2 laser was scaled up to 313 mW for slightly longer pulses of 70 fs at 1049.4 nm, corresponding to a peak power of 51.9 kW and an optical efficiency of 34.7%.

1. Introduction

Strontium fluoride (SrF_2, called *strontiofluorite* in the mineral form) is a cubic (sp. gr. $Fm\bar{3}m$) crystal belonging to the family of alkaline earth fluorides $M^{2+}F_2$ (where M = Ca, Sr, Ba or their mixture) with fluorite (CaF_2) structure. It features wide band gap (~9.7 eV), broad transparency (0.13 – 10 µm), and low refractive index ($n = 1.481$ at ~1 µm) [1], occupying an intermediate place between its CaF_2 and BaF_2 counterparts, and finds applications in UV optical components and thermo-luminescent dosimeters. Due to its congruent melting and a relatively low melting point (about 1477°C), the growth of large volume SrF_2 crystals by the Bridgman-Stockbarger / Czochralski methods is well developed. SrF_2 is a somewhat brittle material being sensitive to thermal shock.

SrF_2 is a suitable laser host material for doping with rare-earth ions (RE^{3+}) [2–5]. It benefits from high thermal conductivity ($\kappa = 9.3$ $Wm^{-1}K^{-1}$) [6], a negative thermo-optic coefficient ($dn/dT = -1.2 \times 10^{-5}$ K^{-1}) [7] leading to a weak thermal lensing, and low phonon energy ($h\nu_{ph} = 285$ cm^{-1}) relevant for suppressing the multi-phonon non-radiative path. Like other fluorite-type crystals, at low doping levels (<0.1 at.%), SrF_2 accommodates RE^{3+} ions in several types of isolated sites (trigonal, C_{3v}, tetragonal, C_{4v}, and cubic, O_h) while at higher doping levels, the dopant ions tend to form clusters ranging from ion pairs (dimers) to large agglomerates leading to significant inhomogeneous spectral broadening of the absorption / emission spectral

#485177 https://doi.org/10.1364/OE.485177
Journal © 2023 Received 16 Jan 2023; revised 11 Mar 2023; accepted 11 Apr 2023; published 3 May 2023

Optics EXPRESS

bands (a "glassy-like" spectroscopic behavior) [8,9]. Similar to other MF_2 crystals, the RE^{3+} ions in SrF_2 crystals exhibit long luminescence lifetimes of 2.24 ms leading to low laser thresholds and good energy storage capabilities.

Ytterbium ions (Yb^{3+}) are known for laser emission around 1 µm owing to the $^2F_{5/2} \rightarrow {}^2F_{7/2}$ electronic transition. They offer a simple energy-level scheme leading to a high slope efficiency and weak heat loading, as well as relatively large Stark splitting of the ground-state ($^2F_{7/2}$) which determines the spectral bandwidths. Yb^{3+}-doped SrF_2 crystals with a doping level of a few at.% (i.e., with the majority of the dopant ions forming clusters) combine good thermal and thermo-optical properties of the host matrix, smooth and broad ("glassy-like") emission / gain profiles of the dopant Yb^{3+} ions, as well as the long luminescence lifetime of the latter [9], making them suitable for high-power / high-energy ultrafast lasers / amplifiers at ~1 µm.

Compared to Yb:CaF_2, Yb:SrF_2 benefits from much higher absorption cross-sections at the zero-phonon line at 976 nm, a slightly longer luminescence lifetime, as well as higher nonlinear refractive index n_2. It is complimentary to Yb:CaF_2 in terms of good thermal properties and a well-developed growth procedure. Camy *et al*. reported on a continuous-wave (CW) Yb:SrF_2 laser pumped by a Ti:Sapphire laser delivering 165 mW at 1046 nm with a slope efficiency of 53% and a laser threshold of 95 mW [9]. The authors also achieved wavelength tuning between 1003 – 1062 nm. Siebold *et al.* developed a high peak power free-running Yb:SrF_2 laser diode-pumped at 940 nm with a tuning range of 73 nm [10]. A Yb:SrF_2 based femtosecond regenerative amplifier produced 325 fs pulses at a repetition rate of 100 Hz with a pulse energy of 1.4 mJ before compression [11]. In 2009, Druon *et al.* reported on a diode-pumped femtosecond Yb:SrF_2 laser mode-locked (ML) by a SEmiconductor Saturable Absorber Mirror (SESAM) delivering 143 fs pulses at 1046.7 nm, with an average output power of 450 mW at a pulse repetition rate of 112.5 MHz [12]. Wu *et al.* developed a diode-pumped SESAM ML Yb,Gd:SrF_2 laser generating 951 fs pulses at 1046 nm at an average output power of 296 mW [13].

Yb:SrF_2 transparent ceramics are also known [14]. Basiev *et al.* reported on a pulsed diode-pumped Yb:(Ca,Sr)F_2 ceramic laser [15]. Doroshenko *et al.* also indicated stimulated-emission from an Yb:SrF_2 ceramic at 1.01 – 1.09 µm without providing details [16].

The promising spectroscopic and thermal properties of the Yb:SrF_2 crystal motivated us to explore its potential for sub-50 fs pulse generation from passively ML lasers. Recently, we have achieved sub-50 fs pulses from a diode-pumped SESAM ML Yb:BaF_2 laser [17]. Note that the growth of high quality Yb:SrF_2 crystals is easier than that of their barium counterparts.

2. Crystal growth and spectroscopy

2.1. Crystal growth

A single-crystal of Yb^{3+}:SrF_2 was grown by the Bridgman-Stockbarger method using a graphite crucible (Φ25 mm, height: 30 mm). The starting reagents were SrF_2 (purity: 4N, Sigma-Aldrich) and YbF_3 obtained by fluorination of an Yb_2O_3 precursor (4N, Alfa Aesar) for attaining higher purity. The initial doping level was 3 at.% Yb^{3+} (with respect to Sr^{2+}). To avoid oxygen pollution potentially causing the formation of O^{2-} assisted optical centers and / or translucent oxyfluoride phases in the SrF_2 crystals, the growth chamber was first sealed to vacuum ($<10^{-5}$ mbar) and then refilled with a mixture of Ar + CF_4 gases. The use of CF_4 is critical to avoid the appearance of Yb^{2+} ions acting as quenching centers.

A mixture of SrF_2 + YbF_3 was introduced into the crucible which was first slightly heated (~30 - 50°C) above the melting point and kept at this temperature for 3 – 4 h to homogenize the melt. The crystal growth started at ~5°C below the melting point and was provided by translating the crucible in a vertical temperature gradient of 30 - 40°C/cm. Once the growth was completed, the crystal was cooled to room temperature (RT, 20°C) within 48 h. A photograph of an as-grown crystal boule is shown in Fig. 1(a). It had cylindric shape (Φ20 mm, length: 25 mm). The crystal was oriented by means of Laue diffraction. A polished crystal sample cut along the [111]

Optics EXPRESS

crystallographic direction providing weak depolarization losses is shown in Fig. 1(b). The crystal was transparent and colorless. The actual Yb^{3+} concentration was determined by Inductively Coupled Plasma Mass Spectrometry (ICP-MS) to be 2.89 at.% (ion density: $N_{Yb} = 5.87 \times 10^{20}$ at/cm^3).

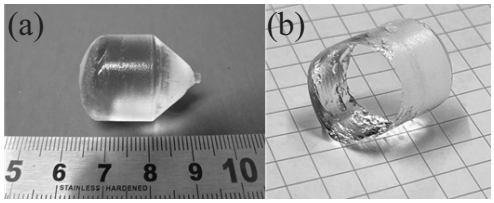

Fig. 1. 2.89 at.% Yb:SrF_2 crystal grown by the Bridgman-Stockbarger method: (a) an as-grown crystal boule; (b) a polished crystal sample oriented along the [111] direction.

2.2. Optical spectroscopy

The transmission spectrum in the 0.2 – 1.2 µm range of a crystal sample (2.6 mm-thick) cut from the central part of the as-grown Yb:SrF_2 crystal boule is shown in Fig. 2(a). It presents an intense Yb^{3+} absorption band around 1 µm (the $^2F_{7/2} \rightarrow {}^2F_{5/2}$ transition). No signs of Yb^{2+} species possessing a characteristic absorption at 0.22 – 0.36 µm [18] are found in the spectrum. The crystal transmission at ~1.2 µm is close to the theoretical one. Note that the UV absorption edge of pure SrF_2, corresponding to its band-gap, appears at ~0.13 µm.

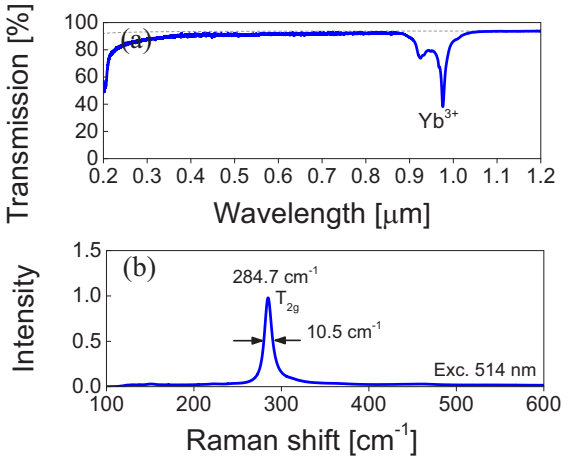

Fig. 2. 2.89 at.% Yb:SrF_2 crystal: (a) transmission spectrum of a polished crystal sample (2.6 mm thick), *grey dashed curve* – theoretical transmission (undoped crystal); (b) RT Raman spectrum, $\lambda_{exc} = 514$ nm.

The unpolarized Raman spectrum of the Yb:SrF_2 crystal is shown in Fig. 2(b). It contains only one peak at 284.7 cm^{-1} (peak width: 10.5 cm^{-1}) typical for the cubic fluorite-type structure (T_{2g} mode) [19]. No other peaks frequently appearing in synthetic SrF_2 crystals and related to defect / F-center modes are observed highlighting the good crystalline quality.

The RT absorption, σ_{abs}, and stimulated-emission (SE), σ_{SE}, spectra for the $^2F_{7/2} \leftrightarrow {}^2F_{5/2}$ Yb^{3+} transition in SrF_2 are shown in Fig. 3(a). The maximum σ_{abs} corresponding to the zero-phonon-line (ZPL) of Yb^{3+} amounts to 0.89×10^{-20} cm^2 at 976.1 nm and the corresponding peak linewidth (full width at half maximum, FWHM) is 8.6 nm. This makes Yb:SrF_2 attractive

Optics EXPRESS

for pumping by commercially available high-power InGaAs laser diodes emitting at ~0.98 µm. The σ_{SE} spectra were calculated using a combination of the Füchtbauer–Ladenburg (F-L) formula and the reciprocity method (RM). In the spectral range where laser operation is expected (at wavelengths well above the ZPL), σ_{SE} amounts to 1.3×10^{-21} cm^2 at ~1049 nm.

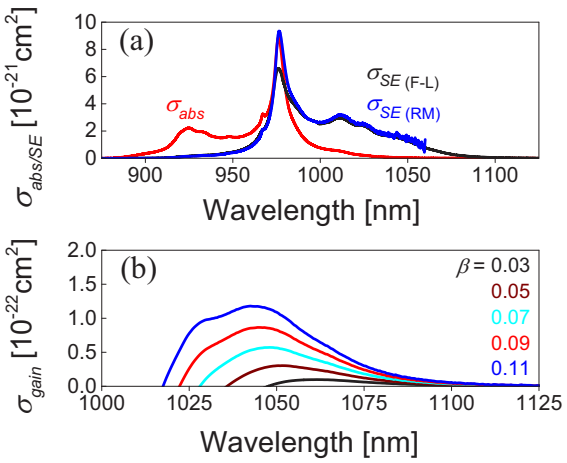

Fig. 3. Transition cross-sections for Yb^{3+} ions in 2.89 at.% Yb:SrF_2 at RT: (a) absorption, σ_{abs}, and stimulated-emission (SE), σ_{SE}, cross-sections; (b) gain cross-sections, $\sigma_{gain} = \beta\sigma_{SE} - (1-\beta)\sigma_{abs}$, $\beta = N_2(^2F_{5/2})/N_{Yb}$ – population inversion ratios $\beta = N_2/N_{Yb}$.

According to the quasi-three-level nature of the Yb laser scheme with reabsorption, the gain cross-section, $\sigma_{gain} = \beta\sigma_{SE} - (1-\beta)\sigma_{abs}$, of Yb:$SrF_2$ was calculated as shown in Fig. 3(b). Here, $\beta = N_2/N_{Yb}$ is the inversion ratio and N_2 is the population of the upper laser level ($^2F_{5/2}$). The gain spectra are smooth and broad exhibiting a "glassy-like" spectroscopic behavior. This is due to the strong inhomogeneous spectral broadening in all fluorite-type crystals (including SrF_2) originating from clustering of the Yb^{3+} dopant ions. With increasing the inversion ratio, the spectral maximum experiences a blue shift, from ~1061 nm for small $\beta = 0.03$ to 1043 nm for higher $\beta = 0.11$. The gain bandwidth (FWHM) for an intermediate $\beta = 0.06$ is 32.5 nm. The broadband gain behavior indicates the high potential of Yb:SrF_2 for broad wavelength tuning and sub-100 fs pulse generation from passively ML lasers.

The RT luminescence lifetime of the upper laser level ($^2F_{5/2}$) of Yb^{3+} ions in SrF_2 was measured using a finely powdered crystalline sample to avoid the effect of radiation trapping (reabsorption), see Fig. 4. The Yb^{3+} ion luminescence exhibits a single-exponential decay with a characteristic lifetime $\tau_{lum} = 2.24$ ms. This value agrees well with the radiative lifetime $\tau_{rad} = 2.25 \pm 0.1$ ms used for calculating the σ_{SE} spectra via the F-L formula.

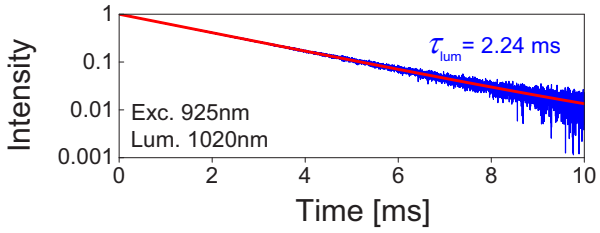

Fig. 4. RT luminescence decay curve (blue) of the 2.89 at.% Yb:SrF_2 crystal, $\lambda_{exc} = 925$ nm, $\lambda_{lum} = 1020$ nm, *red line* – single-exponential fit.

Optics EXPRESS

The low-temperature (LT, 10 K) absorption and emission spectra of Yb^{3+} ions in SrF_2 are shown in Fig. 5. The electronic transitions of Yb^{3+} ions in clusters were assigned following the previous work on 5 at.% Yb:CaF_2 [20]. The Stark sub-levels of the ground-state ($^2F_{7/2}$) were labeled as $i = 0, 1, 2, 3$ and those of the excited-state ($^2F_{5/2}$) – as $j = 0', 1', 2'$. The experimental crystal-field splitting is $^2F_{7/2}$ = [0, 91, 490, 672] cm^{-1} and $^2F_{5/2}$ = [10221, 10375, 10872] cm^{-1} corresponding to the partition functions $Z_1 = 1.766$ and $Z_2 = 1.509$, so that their ratio $Z_1/Z_2 = 1.17$. The ZPL corresponding to transitions between the lowest sub-levels of the two manifolds has an energy E_{ZPL} of 10221 cm^{-1}. These parameters were used for calculating the σ_{SE} spectra via RM.

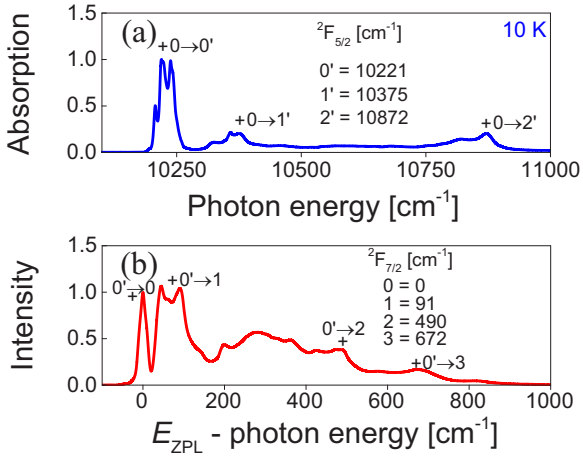

Fig. 5. LT (10 K) absorption (a) and emission (b) spectra of Yb^{3+} ions in the 2.89 at.% Yb:SrF_2 crystal, "+" mark electronic transitions assigned to Yb^{3+} ion clusters.

3. Laser set-up

The schematic of the Yb:SrF_2 laser is shown in Fig. 6. A cubic laser element was cut from the as-grown bulk 2.89 at.% Yb:SrF_2 crystal for light propagation along the [111] direction [21] having an aperture of 3 mm × 3 mm and a thickness of 3 mm. It was polished to laser-grade quality from both sides with good parallelism and mounted in a passively cooled copper holder using Indium foil. The sample was placed at Brewster's angle between the two concave folding mirrors M_1 and M_2 (radius of curvature, RoC = -100 mm) in an astigmatically compensated X-shaped standing-wave cavity. The pump source was a spatially single-mode, fiber-coupled InGaAs laser diode delivering a maximum output power of 1.29 W at 976 nm (the emission wavelength was locked with a fiber Bragg grating (FBG) and the spectral linewidth (FWHM) was ~0.2 nm). The pump radiation was unpolarized. The measured beam propagation factor M^2 of the pump radiation at the maximum output power was ~1.02. The pump beam was collimated and focused into the laser crystal through the M_1 mirror via an aspherical lens L_1 (focal length: $f = 26$ mm) and a spherical focusing lens L_2 ($f = 100$ mm) yielding a beam waist (radius) of 18.7 µm × 33.5 µm in the sagittal and tangential planes, respectively.

The CW laser performance was evaluated in a four-mirror cavity without implementing the saturable absorber (SA) and the DMs. One cavity arm was terminated by a flat end mirror M_3 and the other cavity arm – by a plane-wedged output coupler (OC) with a transmission at the laser wavelength T_{OC} in the range of 0.4% - 7.5%. The radius of the fundamental laser cavity mode inside the Yb:SrF_2 crystal was estimated by the ABCD method to be 22.7 µm × 33.0 µm in the sagittal and tangential planes, respectively. The measured single-pass pump absorption

Optics EXPRESS

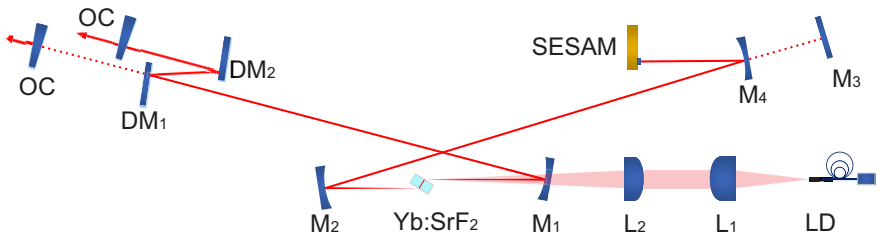

Fig. 6. The schematic of the Yb:SrF_2 laser. LD: fiber-coupled laser diode; L_1: aspherical collimating lens; L_2: spherical focusing lens; M_1, M_2 and M_4: curved mirrors (RoC = -100 mm); M_3: flat end mirror for CW laser operation; DM_1 and DM_2: flat dispersive mirrors; OC: output coupler; SESAM: SEmiconductor Saturable Absorber Mirror.

under lasing conditions decreased with the output-coupling in the range of 84% - 67% due to the ground-state bleaching.

For passively ML operation, the flat end mirror M_3 was substituted by a curved mirror M_4 (RoC = -100 mm) for creating a second beam waist on the SESAM with a calculated beam radius of ~78 μm to ensure its efficient bleaching. A commercial SESAM (BATOP, GmbH) was implemented. Its parameters at ~1 μm were as follows: a modulation depth of 3%, a non-saturable loss of 2%, a saturation fluence of 45 μJ/cm^2 and a relaxation time of ~1 ps. Two flat dispersive mirrors (DM_1 and DM_2) with a negative group delay dispersion (GDD) per bounce of -250 fs^2 were implemented in the other cavity arm to compensate the dispersion from the SrF_2 crystal (20.4 fs^2/mm at 1050 nm) and to balance the self-phase modulation (SPM) for soliton pulse shaping. The geometrical cavity length of the ML Yb:SrF_2 laser was 1.976 m, corresponding to a pulse repetition rate of ~75.9 MHz.

4. Continuous-wave laser operation

In the CW regime, the maximum output power of the Yb:SrF_2 laser amounted to 704 mW at 1048 nm at an absorbed pump power P_{abs} of 969 mW corresponding to a slope efficiency η of 77.2% and a laser threshold of 64 mW (for 2.5% OC), Fig. 7(a). The laser threshold gradually increased with the output coupling, from 36 mW (T_{OC} = 0.4%) to 131 mW (T_{OC} = 7.5%). The

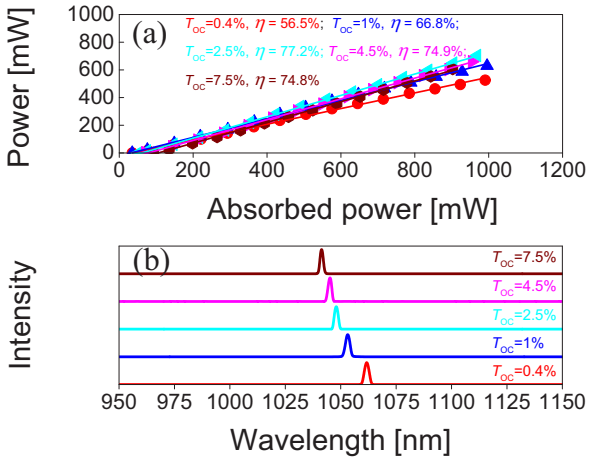

Fig. 7. CW diode-pumped Yb:SrF_2 laser: (a) input - output dependences for different OCs, η – slope efficiency; (b) typical spectra of laser emission.

Optics EXPRESS

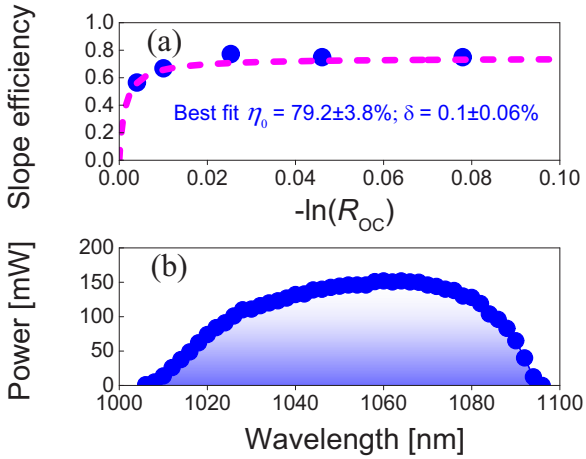

Fig. 8. CW diode-pumped Yb:SrF_2 laser: (a) Caird analysis: slope efficiency *vs.* $R_{OC} = 1 - T_{OC}$; (b) tuning curve obtained with a Lyot filter and $T_{OC} = 0.4\%$.

laser wavelength experienced a monotonous blue-shift with increasing the output coupling in the range of 1023.2 – 1058.7 nm, as shown in Fig. 7(b). This behavior is typical for quasi-three-level Yb lasers with inherent reabsorption at the laser wavelength.

The Caird analysis was applied by fitting the measured laser slope efficiency as a function of the output coupler reflectivity, $R_{OC} = 1 - T_{OC}$ [22]. The total round-trip cavity losses δ (reabsorption losses excluded), as well as the intrinsic slope efficiency η_0 (accounting for the mode-matching and the quantum efficiency) were estimated yielding $\eta_0 = 79.2 \pm 3.8\%$ and $\delta = 0.1 \pm 0.06\%$, as shown in Fig. 8(a). The low value of δ evidences the good optical quality of the laser crystal.

The wavelength tuning of the Yb:SrF_2 laser in the CW regime was studied by inserting a 2-mm thick quartz plate acting as a Lyot filter at Brewster's angle in the cavity arm terminated by the OC. A lower T_{OC} of 0.4% was used and the incident pump power was 800 mW. The laser wavelength was continuously tunable between 1006 and 1095 nm, i.e., across 89 nm at the zero-power-level, Fig. 8(b).

5. SESAM mode-locked laser operation

The SESAM was implemented to start and stabilize the soliton ML operation of the Yb:SrF_2 laser. A total round-trip negative GDD of -1000 fs^2 was introduced by using the two flat DMs (DM_1 – DM_2), see Fig. 6. After careful cavity alignment, stable and self-starting ML operation was readily achieved with a 4% OC. The measured optical spectrum of the laser had a FWHM of 17 nm assuming a $sech^2$-shaped profile at a central wavelength of 1049.4 nm, Fig. 9(a). The second-harmonic generation (SHG)-based intensity autocorrelation trace was well fitted with a $sech^2$-shaped temporal profile giving a pulse duration (FWHM) of 70 fs corresponding to a time-bandwidth-product (TBP) of 0.324, see Fig. 9(b). An average output power of 313 mW was obtained at P_{abs} of 902 mW for a pulse repetition rate of 75.9 MHz, corresponding to an optical efficiency of 34.7% and a peak power of 51.9 kW. The inset in Fig. 9(b) shows the measured intensity autocorrelation trace on a long-time span of 50 ps indicating single-pulse CW-ML operation free of multiple pulse instabilities.

Shorter pulses could be achieved by using a smaller output coupling of 2.5%. The Yb:SrF_2 laser delivered pulses with a spectral bandwidth of 21 nm at a central wavelength of 1055.2 nm (assuming a $sech^2$-shaped profile), Fig. 10(a). The excellent fit of the recorded intensity autocorrelation trace using a $sech^2$-shaped temporal profile resulted in an estimated pulse duration

Optics EXPRESS

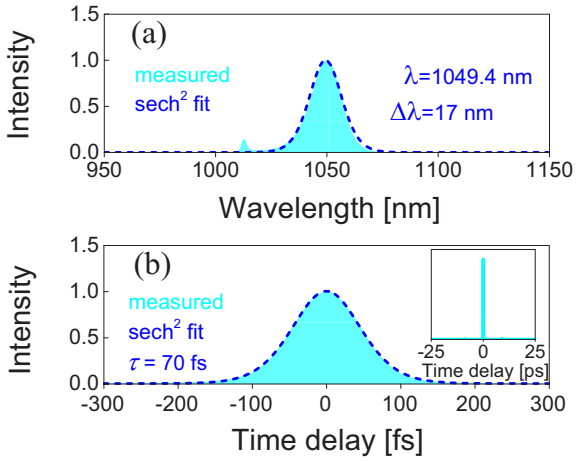

Fig. 9. SESAM ML Yb:SrF_2 laser with $T_{OC} = 4\%$. (a) Optical spectrum and (b) SHG-based intensity autocorrelation trace. *Inset*: autocorrelation trace on a time span of 50 ps.

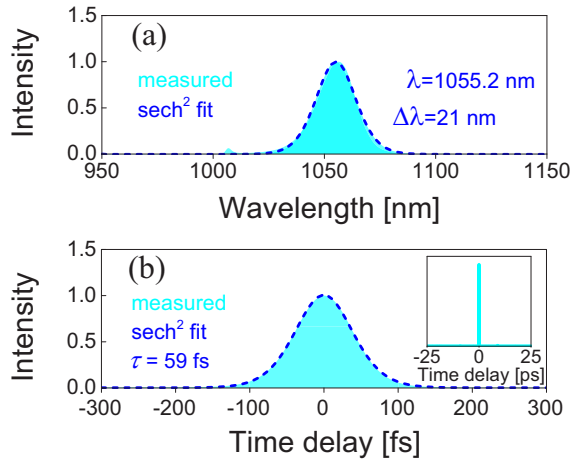

Fig. 10. SESAM ML Yb:SrF_2 laser with $T_{OC} = 2.5\%$. (a) Optical spectrum and (b) SHG-based intensity autocorrelation trace. *Inset*: autocorrelation trace on a time span of 50 ps.

of 59 fs, see Fig. 10(b). The 50-ps long-time scale autocorrelation trace revealed single-pulse mode-locking, see the inset in Fig. 10(b). The corresponding TBP was 0.318 being very close to the Fourier-transform-limited value of 0.334. The average output power dropped to 262 mW at P_{abs} of 795 mW for the same pulse repetition rate of 75.9 MHz, corresponding to an optical efficiency of 32.9% and a peak power of 51.5 kW.

The shortest pulses with ultimate stability were achieved using a 1% OC. Assuming a $sech^2$-shaped spectral profile, an emission bandwidth of 25 nm was observed at a central wavelength of 1057 nm, see Fig. 11(a). Figure 11(b) shows the recorded intensity autocorrelation trace for the shortest pulses. The curve was well fitted with a $sech^2$-shape temporal profile, yielding 49 fs for the pulse duration. This corresponds to a TBP of 0.329 again being very close to the Fourier-transform-limit. Single-pulse CW mode-locking was also confirmed by a long time-scale intensity autocorrelation trace, see the inset in Fig. 11(b). The average output power further

Optics EXPRESS

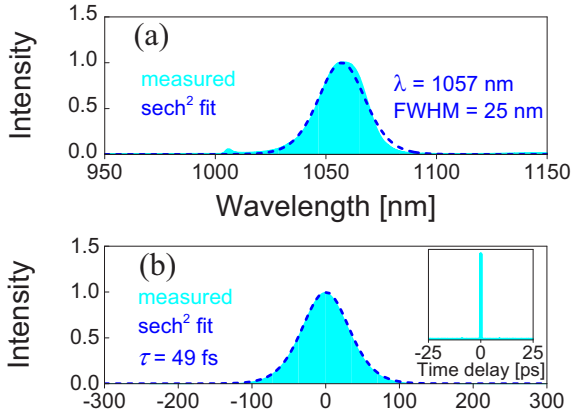

Fig. 11. SESAM ML Yb:SrF_2 laser with T_{OC} = 1%. (a) Laser spectrum and (b) SHG-based intensity autocorrelation trace. *Inset*: autocorrelation trace on a time span of 50 ps.

dropped to 117 mW at P_{abs} of 856 mW, which corresponded to an optical efficiency of 13.7% and a peak power of 27.7 kW.

The radio-frequency (RF) spectra of the shortest pulses were recorded to confirm the stability of the ML operation in different frequency span ranges, as shown in Fig. 12. The recorded fundamental beat note located at 75.9 MHz exhibited a high extinction ratio of >76 dBc above carrier, see Fig. 12(a). The measured uniform harmonics on a 1-GHz frequency span again revealed high stability of the single-pulse ML operation, see Fig. 12(b).

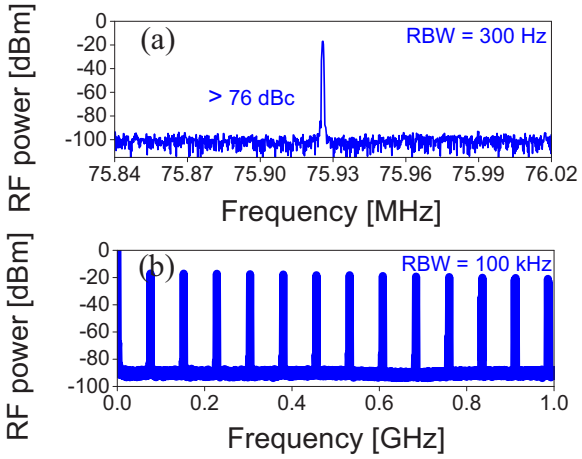

Fig. 12. RF spectra of the SESAM mode-locked Yb:SrF_2 laser: (a) Fundamental beat note at 75.9 MHz recorded with a resolution bandwidth (RBW) of 300 Hz, and (b) Harmonics on a 1-GHz frequency span recorded with an RBW of 100 kHz. T_{OC} = 1%.

To confirm the pulse shaping mechanism, the far-field beam profiles of the Yb:SrF_2 laser both in the CW and ML regimes were recorded with an IR camera placed at ~1.2 m from the OC. It was relatively easy to switch between the CW and ML regimes just by a slight cavity misalignment. Almost unchanged beam diameters in the far-field were observed during such switching, see Fig. 13. This observation in combination with the excellent $sech^2$-shaped spectral and temporal profiles of the shortest pulses indicates that soliton mode-locking was the dominant pulse shaping mechanism rather than Kerr-lens mode-locking. This conclusion is in line with the

Optics EXPRESS

relatively small value of the nonlinear refractive index n_2 of strontium fluoride at ~1 μm (0.91 – 1.34×10^{-20} m^2/W [23]), resulting in a weak nonlinear amplitude modulation for a 3 mm-thick laser crystal.

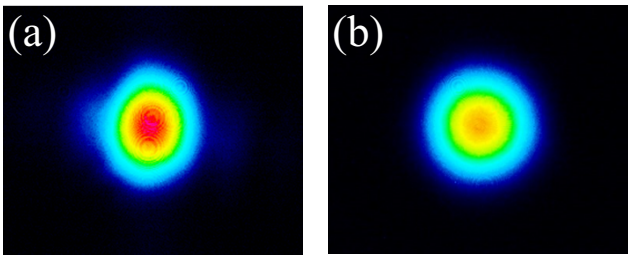

Fig. 13. Measured far-field beam profiles of the diode-pumped SESAM ML Yb:SrF_2 laser: (a) CW and (b) SESAM ML operation.

The weak satellite peaks observed in the spectra of the mode-locked Yb:SrF_2 laser around 1005 nm are assigned to uncompensated intracavity GDD at the short-wave spectral wing and non-optimized spectral reflectivity of the cavity mirrors. A similar phenomenon was previously observed for a SESAM mode-locked Yb:$CaGdAlO_4$ laser with a prism pair for the dispersion management [24], and later explained by Sévillano *et al*. [25].

6. Conclusion

To conclude, ytterbium-doped strontium fluoride (Yb:SrF_2) is a promising crystal for broadly tunable lasers and especially power-scalable ultrafast (sub-100 fs) oscillators emitting around 1 μm. In the present work, we report on the sub-50 fs pulse generation from a diode-pumped SESAM mode-locked 2.89 at.% Yb:SrF_2 laser. By using a high-brightness pump source (a cost-effective single-mode fiber-coupled InGaAs laser diode), a commercial SESAM for initiating and sustaining the mode-locking operation, soliton pulses as short as 49 fs were generated at a central wavelength of 1057 nm corresponding to an average output power of 117 mW at a pulse repetition rate of ~75.9 MHz. Our laser results indicate the potential of Yb:SrF_2 crystals with optimized Yb^{3+} ion doping levels and thickness for further power scaling and pulse shortening via the Kerr-lens mode-locking technique as demonstrated previously for Yb:CaF_2 [26,27].

Funding. National Natural Science Foundation of China (61975208, 61905247, U21A20508); Sino-German Scientist Cooperation and Exchanges Mobility Program (M-0040); National Key Research and Development Program of China (2021YFB3601504); Agencia Estatal de Investigación (PID2019-108543RB-I00).

Acknowledgment. Xavier Mateos acknowledges the Serra Húnter program.

Disclosures. The authors declare no conflicts of interest.

Data availability. Data underlying the results presented in this paper are not publicly available at this time but may be obtained from the authors upon reasonable request.

References

1. H. H. Li, "Refractive index of alkaline earth halides and its wavelength and temperature derivatives," J. Phys. Chem. Ref. Data **9**(1), 161–290 (1980).
2. F. Druon, S. Ricaud, D. N. Papadopoulos, A. Pellegrina, P. Camy, J. L. Doualan, R. Moncorgé, A. Courjaud, E. Mottay, and P. Georges, "On Yb:CaF_2 and Yb:SrF_2: review of spectroscopic and thermal properties and their impact on femtosecond and high power laser performance," Opt. Mater. Express **1**(3), 489–502 (2011).
3. W. Ma, X. Qian, J. Wang, J. Liu, X. Fan, J. Liu, L. Su, and J. Xu, "Highly efficient dual-wavelength mid-infrared CW laser in diode end-pumped Er:SrF_2 single crystals," Sci. Rep. **6**(1), 36635 (2016).
4. T. T. Basiev, M. E. Doroshenko, V. A. Konyushkin, and V. V. Osiko, "SrF_2:Nd^{3+} laser fluoride ceramics," Opt. Lett. **35**(23), 4009–4011 (2010).
5. A. Sottile, E. Damiano, M. Rabe, R. Bertram, D. Klimm, and M. Tonelli, "Widely tunable, efficient 2 μm laser in monocrystalline Tm^{3+}:SrF_2," Opt. Express **26**(5), 5368–5380 (2018).

Optics EXPRESS

6. P. A. Popov, P. P. Fedorov, V. A. Konyushkin, A. N. Nakladov, S. V. Kuznetsov, V. V. Osiko, and T. T. Basiev, "Thermal conductivity of single crystals of $Sr_{1-x}Yb_xF_{2+x}$ solid solution," Dokl. Phys. **53**(8), 413–415 (2008).
7. J. Boudeile, J. Didierjean, P. Camy, J. L. Doualan, A. Benayad, V. Ménard, R. Moncorgé, F. Druon, F. Balembois, and P. Georges, "Thermal behaviour of ytterbium-doped fluorite crystals under high power pumping," Opt. Express **16**(14), 10098–10109 (2008).
8. V. Petit, P. Camy, J.-L. Doualan, X. Portier, and R. Moncorgé, "Spectroscopy of Yb^{3+}:CaF_2: from isolated centers to clusters," Phys. Rev. B **78**(8), 085131 (2008).
9. P. Camy, J. L. Doualan, A. Benayad, M. Von Edlinger, V. Ménard, and R. Moncorgé, "Comparative spectroscopic and laser properties of Yb^{3+}-doped CaF_2, SrF_2 and SrF_2 single crystals," Appl. Phys. B **89**(4), 539–542 (2007).
10. M. Siebold, J. Hein, M. C. Kaluza, and R. Uecker, "High-peak-power tunable laser operation of Yb:SrF_2," Opt. Lett. **32**(13), 1818–1820 (2007).
11. S. Ricaud, P. Georges, P. Camy, J. L. Doualan, R. Moncorge, A. Courjaud, E. Mottay, and F. Druon, "Diode-pumped regenerative Yb:SrF_2 amplifier," Appl. Phys. B **106**(4), 823–827 (2012).
12. F. Druon, D. N. Papadopoulos, J. Boudeile, M. Hanna, P. Georges, A. Benayad, P. Camy, J. L. Doualan, V. Menard, and R. Moncorge, "Mode-locked operation of a diode-pumped femtosecond Yb:SrF_2 laser," Opt. Lett. **34**(15), 2354–2356 (2009).
13. Y. Wu, Z. Zou, C. Wang, J. Liu, L. Zheng, and L. Su, "Broadly tunable and passively mode-locked operations of Yb^{3+},Gd^{3+}:SrF_2 laser," IEEE J. Select. Topics Quantum Electron. **25**(4), 1–5 (2019).
14. Y. Gao, B. Mei, W. Li, Z. Zhou, and Z. Liu, "Effect of Yb^{3+} concentration on microstructure and optical properties of Yb:SrF_2 transparent ceramics," Opt. Mater. (Amsterdam, Neth.) **105**, 109869 (2020).
15. T. T. Basiev, M. E. Doroshenko, P. P. Fedorov, V. A. Konyushkin, S. V. Kuznetsov, V. V. Osiko, and M. S. Akchurin, "Efficient laser based on CaF_2-SrF_2-YbF_3 nanoceramics," Opt. Lett. **33**(5), 521–523 (2008).
16. M. E. Doroshenko, A. A. Demidenko, P. P. Fedorov, E. A. Garibin, P. E. Gusev, H. Jelinkova, V. A. Konyshkin, M. A. Krutov, S. V. Kuznetsov, V. V. Osiko, and P. A. Popov, "Progress in fluoride laser ceramics," Phys. Status Solidi C **10**(6), 952–957 (2013).
17. W.-Z. Xue, Z.-L. Lin, H.-J. Zeng, G. Zhang, P. Loiko, L. Basyrova, A. Benayad, P. Camy, V. Petrov, X. Mateos, L. Wang, and W. Chen, "Diode-pumped mode-locked Yb:BaF_2 laser," Opt. Express **30**(9), 15807–15818 (2022).
18. B. Moine, B. Courtois, and C. Pedrini, "Luminescence and photoionization processes of Yb^{2+} in CaF_2, SrF_2 and BaF_2," J. Phys. (Paris) **50**(15), 2105–2119 (1989).
19. A. R. Gee, D. C. O'Shea, and H. Z. Cummins, "Raman scattering and fluorescence in calcium fluoride," Solid State Commun. **4**(1), 43–46 (1966).
20. M. Ito, C. Goutaudier, Y. Guyot, K. Lebbou, T. Fukuda, and G. Boulon, "Crystal growth, Yb^{3+} spectroscopy, concentration quenching analysis and potentiality of laser emission in $Ca_{1-x}Yb_xF_{2+x}$," J. Phys.: Condens. Matter **16**(8), 1501–1521 (2004).
21. K. Genevrier, D. N. Papadopoulos, M. Besbes, P. Camy, J. L. Doualan, R. Moncorgé, P. Georges, and F. Druon, "Thermally-induced-anisotropy issues in oriented cubic laser crystals, the cryogenically cooled Yb:CaF_2 case," Appl. Phys. B **124**(11), 209 (2018).
22. J. A. Caird, S. A. Payne, P. R. Staver, A. Ramponi, and L. Chase, "Quantum electronic properties of the $Na_3Ga_2Li_3F_{12}$:Cr^{3+} laser," IEEE J. Quantum Electron. **24**(6), 1077–1099 (1988).
23. Y. Guo, S. Lu, L. Su, C. Zhao, H. Zhang, and S. Wen, "Z-scan measurement of the nonlinear refractive index of Nd^{3+}, Y^{3+}-codoped CaF_2 and SrF_2 crystals," Appl. Opt. **54**(4), 953–958 (2015).
24. Y. Zaouter, J. Didierjean, F. Balembois, G. L. Leclin, F. Druon, P. Georges, J. Petit, P. Goldner, and B. Viana, "47-fs diode-pumped Yb^{3+}:$CaGdAlO_4$ laser," Opt. Lett. **31**(1), 119–121 (2006).
25. P. Sévillano, P. Georges, F. Druon, D. Descamps, and E. Cormier, "32-fs Kerr-lens mode-locked Yb:$CaGdAlO_4$ oscillator optically pumped by a bright fiber laser," Opt. Lett. **39**(20), 6001–6004 (2014).
26. G. Machinet, P. Sevillano, F. Guichard, R. Dubrasquet, P. Camy, J. L. Doualan, R. Moncorgé, P. Georges, F. Druon, D. Descamps, and E. Cormier, "High-brightness fiber laser-pumped 68 fs-2.3 W Kerr-lens mode-locked Yb:CaF_2 oscillator," Opt. Lett. **38**(20), 4008–4010 (2013).
27. P. Sevillano, G. Machinet, R. Dubrasquet, P. Camy, J.-L. Doualan, R. Moncorge, P. Georges, F. P. Druon, D. Descamps, E. E. D. H. G. Cormier, and P. Moulton, "Sub-50 fs, Kerr-lens mode-locked Yb:CaF2 laser oscillator delivering up to 2.7 W," in *Advanced Solid-State Lasers Congress* (Optical Society of America, Paris), p. AF3A.6 (2013).